OPEN ACCESS
IOP Publishing | Songshan Lake Materials Laboratory
Materials Futures
Mater. Futures 2 (2023) 032101 (17pp)
https://doi.org/10.1088/2752-5724/acd56c

Topical Review

The stability of inorganic perovskite solar cells: from materials to devices

Bingcheng Yu[1,2], Shan Tan[1,3], Dongmei Li[1,4,5,*] and Qingbo Meng[1,3,5,*]

[1] Beijing National Laboratory for Condensed Matter Physics, Renewable Energy Laboratory, Institute of Physics, Chinese Academy of Sciences (CAS), Beijing 100190, People's Republic of China
[2] Huairou Division, Institute of Physics, Chinese Academy of Sciences, Beijing 101407, People's Republic of China
[3] College of Materials Science and Opto-Electronic Technology, University Chinese Academy of Sciences, Beijing 100049, People's Republic of China
[4] School of Physical Sciences, University of Chinese Academy of Sciences, Beijing 100049, People's Republic of China
[5] Songshan Lake Materials Laboratory, Dongguan, Guangdong 523808, People's Republic of China

E-mail: dmli@iphy.ac.cn and qbmeng@iphy.ac.cn

Received 22 March 2023, revised 8 May 2023
Accepted for publication 15 May 2023
Published 9 June 2023

Abstract

Inorganic halide perovskite solar cells (IHPSCs) have become one of the most promising research hotspots due to to the excellent light and thermal stabilities of inorganic halide perovskites (IHPs). Despite rapid progress in cell performance in very recent years, the phase instability of IHPs easily occurs, which will remarkably influence the cell efficiency and stability. Much effort has been devoted to solving this issue. In this review, we focus on representative progress in the stability from IHPs to IHPSCs, including (i) a brief introduction of inorganic perovskite materials and devices, (ii) some new additives and fabrication methods, (iii) thermal and light stabilities, (iv) tailoring phase stability, (v) optimization of the stability of inorganic perovskite solar cells and (vi) interfacial engineering for stability enhancement. Finally, perspectives will be given regarding future work on highly efficient and stable IHPSCs. This review aims to provide a thorough understanding of the key influential factors on the stability of materials to highly efficient and stable IHPSCs.

Keywords: inorganic halide perovskites, inorganic halide perovskite solar cells, light stability, thermal stability, phase instability

1. Introduction

In recent years, perovskite solar cells (PSCs) based on organic–inorganic hybrid lead halide light absorbers have become one of the most focused research fields in the photovoltaic field due to their outstanding photoelectric conversion properties [1–4]. Since the first PSC was reported by Miyasaka *et al* in 2009, the power conversion efficiency (PCE) of PSCs has already climbed to 25.7%, comparable with that of the state-of-the-art crystalline silicon solar cells [5–13]. To date, the PSCs with higher PCEs over 22% have all been based on organic–inorganic hybrid perovskite materials, which exhibit a 3D crystal structure with a general chemical formula of ABX_3, where A is a monovalent cation, such as methylammonium ($CH_3NH_3^+$, MA^+) and

* Authors to whom any correspondence should be addressed.

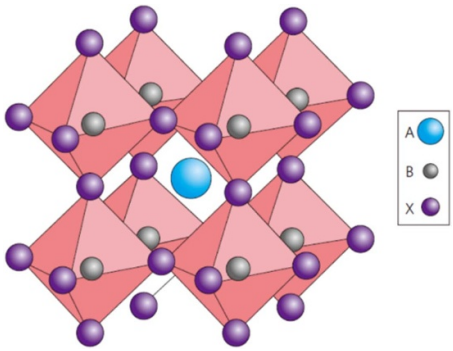

Figure 1. Crystal structure of a typical black phase ABX_3 perovskite. Reproduced from [14] with permission from Springer Nature.

formamidinium ($HC(CH_2)_2^+$, FA^+), B is a divalent cation, such as Pb^{2+} and Sn^{2+}, and X is a halide ion, such as I^-, Br^-, and Cl^-, as shown in figure 1 [14]. However, the PSCs based on organic–inorganic hybrid perovskite face a series of stability issues. For example, compositional and structural degradation, thermal and chemical instabilities derived from phase transformations (i.e. moisture or oxygen) and UV light instability [15–18]. Extensive attention has been focussed on improving stabilities of PSCs to promote its commercial application. For example, introducing additives to control the perovskite crystallinity and to reduce defects and grain boundaries, developing interfacial layers to passivate interface defects, or designing new materials from the perovskite itself, hole transporting materials to carbon electrodes [13, 19–31]. In addition to organic ammonium cations, inorganic cations, such as Cs^+, can also be used to construct a 3D perovskite with Pb^{2+} and halides, thus forming all-inorganic perovskite materials. For example, $CsPbI_3$, $CsPbBr_3$ and their alloying compounds [32–34]. These materials also exhibit a high visible-light absorption coefficient, thus being able to be used as a light absorber for the cell [33]. Due to a much lower volatility and reduced rotation freedom of the A-site inorganic cation, thermal and light illumination stabilities of all-inorganic perovskite materials have been significantly improved [35–39]. Thus, it is generally considered that all-inorganic PSCs have provided more alternative approaches for overcoming the stability issue of PSCs.

The appearance of inorganic perovskite materials could date to 1893. However, it was not until 2015 that $CsPbI_3$ and $CsPbBr_3$ were first assembled into photovoltaic devices (so-called inorganic halide perovskite solar cells (IHPSCs)) [32, 40]. Compared to hybrid perovskite cells, these IHPSCs exhibit superior operational stability under continuous light illumination and electric field [38, 41, 42]. By in-depth study of the composition engineering, crystallization control and interface engineering of IHPSCs, its PCEs have already climbed to 21% [39, 41–47]. These achievements have been mainly dependent on the development of inorganic perovskite materials and further understanding device operation principles. In addition to $CsPbX_3$ perovskites, other all-inorganic perovskites have also been developed [48, 49]. In recent years, the phase stability issue of the all-inorganic perovskite has been of great concern, and numerous efforts have been made to improve this stability [37].

In this review, we focus on the important progress related to stabilities from inorganic halide perovskites (IHPs) to IHPSCs. Meanwhile, more attention is also paid to phase instability and accurate control. Finally, perspectives for future development of highly efficient and stable IHPSCs are presented.

2. Inorganic perovskite materials and devices

In this section, the crystal structure and properties of IHPs are presented first. We then provide a brief introduction to the architectures and fabrication methods of IHPSCs.

2.1. Structure and properties of IHPs

Cs-based IHPs are described by the chemical formula $CsBX_3$ ($B = Pb^{2+}$, Mn^{2+}, Sn^{2+}, etc, $X = Cl^-$, Br^-, I^-), where Cs^+ occupies a corner of a unit cell with 12-fold coordination, B is a divalent metal cation sitting in a body-centered position with six-fold coordination, and X is a halogen in a face-centered position, as depicted in figure 1 [14]. Generally, the crystal structure of the $CsBX_3$ is determined by two important empirical parameters, Goldschmidt's tolerance factor t and the octahedral factor μ, which are defined as follows [50, 51]:

$$t = (r\mathrm{Cs} + r\mathrm{X})/\sqrt{2}(r\mathrm{B} + r\mathrm{X}),$$

$$\mu = r\mathrm{Cs}/r\mathrm{X},$$

where r represents the ionic radius of the corresponding cations and anions. To the phase-stable halide perovskites, the proper range of the tolerance factor is $0.8 < t < 1$. Furthermore, μ in the range from 0.4–0.9 ensures the formation of stable $[BX_6]^{4-}$ octahedra. Although the ionic radius of Cs^+ is smaller than those of organic MA^+ and FA^+ cations, their overall phase stability is not far from the above-mentioned range, as shown in figure 2(a). Due to these structural limitations (simultaneously satisfying the t and μ conditions), when the A site is occupied by Cs^+, the combination numbers of B and X ions are very limited to 3D perovskite, as shown in figure 2(b). Under an ideal situation, if the void size determined by $[BX_6]^{4-}$ octahedra matches well with the Cs^+ size, the ideal cubic perovskite phase with $t = 1$ is obtained. Unfortunately, the Cs^+ size is smaller than the void size, leading to $t < 1$. For example, the reported tolerance factor of $CsPbI_3$ is 0.807, which has to undergo a higher octahedral rotation distortion in comparison to $CsPbBr_3$ with a higher t value ($t = 0.824$). In other words, the $[PbX_6]^{4-}$ octahedron will rotate and tilt to reduce the extra space around the Cs^+ cation. In addition, taking

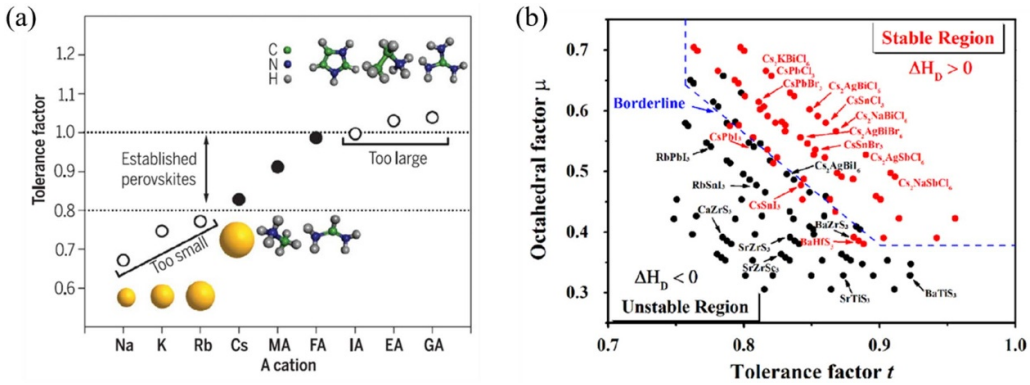

Figure 2. (a) Tolerance factor of $APbI_3$ perovskites with different cations. From [50], reprinted with permission from AAAS. (b) Map of (t, μ) for 138 perovskites with different compounds. Reprinted with permission from [51]. Copyright (2017) American Chemical Society.

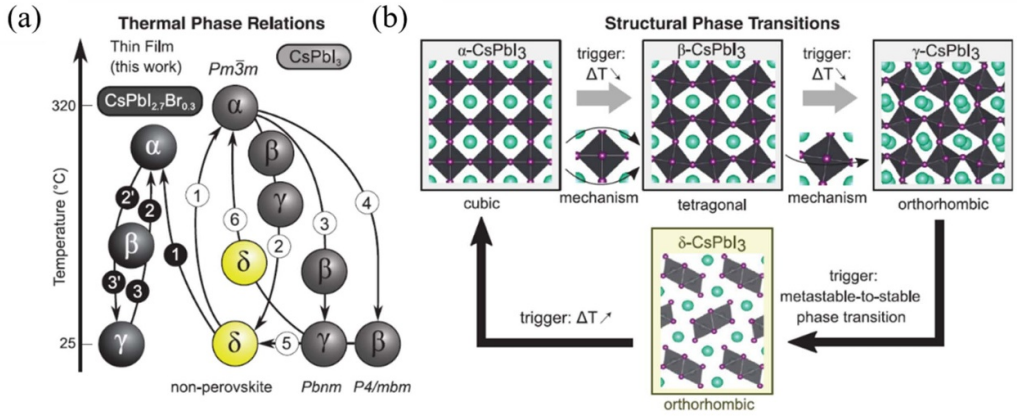

Figure 3. (a) Comparison of the thermal phase relationship of $CsPbI_3$ and the phase behavior of strained $CsPbI_{2.7}Br_{0.3}$ thin films. From [52], reprinted with permission from AAAS. (b) Crystal structure and relative phase transition process of different phases. From [52], reprinted with permission from AAAS.

$CsPbI_3$ as an example, a thermodynamically stable yellow δ-phase (non-perovskite) at room temperature will transform into an optically active black perovskite phase through a reversible high-temperature phase: α (cubic), β (tetragonal) and γ (orthorhombic). This process involves the rotation of the $[PbI_6]^{4-}$ octahedron. Thermal phase relations of $CsPbI_3$ are depicted in figure 3 [52]. The term 'black' is used to collectively define (*pseudo*-) cubic phases, as they typically exhibit similar optoelectronic properties. However, the black phase is unstable at room temperature.

In order to predict the optoelectronic properties of IHPs, density functional theory has been employed to calculate their electronic structures. Considering the relativistic correction and spin–orbit interaction, the following two conclusions were obtained. First, the halide has little effect on the specific energy band structure, except for bandgap values, and second, $CsPbX_3$ perovskites show a direct band gap, indicating that they have broad application prospects in optoelectronics. In addition, Cs^+, as for the organic A cation, has little direct effect on the electronic structure near the band edge, although it can indirectly affect the tilting of the $[PbX_6]^{4-}$ octahedral. Therefore, the excitation and recombination of electrons and excitons are confined within the $[PbV_6]^{4-}$ octahedra (figure 4(a)) [53]. Furthermore, Nicholas *et al* calculated the effective mass (μ) and exciton binding (R^*) energy of $CsPbX_3$ perovskites by performing magneto transmission measurements, and the values of these parameters increased with the band-gap energy increasing. In other words, these parameters are related to heavy metal halides. At the same time, the dielectric constant from experiments shows that, when the movement of organic cations is frozen at low temperatures, the dielectric screening mechanism of hybrid and inorganic perovskites is basically the same, which is dominated by the relative motion of atoms within the $[PbI_6]^{4-}$ octahedra cage, as shown in figure 4(b) [54].

Whether a semiconductor material is suitable for a solar energy harvester depends on the following photophysical parameters: band gap, light absorption coefficient, carrier diffusion length. For an ideal single-junction solar cell system, the relationship between E_g and its theoretical efficiency limit follows the Shockley–Queisser (SQ) limit. For $CsPbX_3$, the light absorption range of the material is determined by its band gap from 1.73–2.31 eV, which is controllable by adjusting the ratio of the halogen, as shown in figure 5(a) [34]. The light

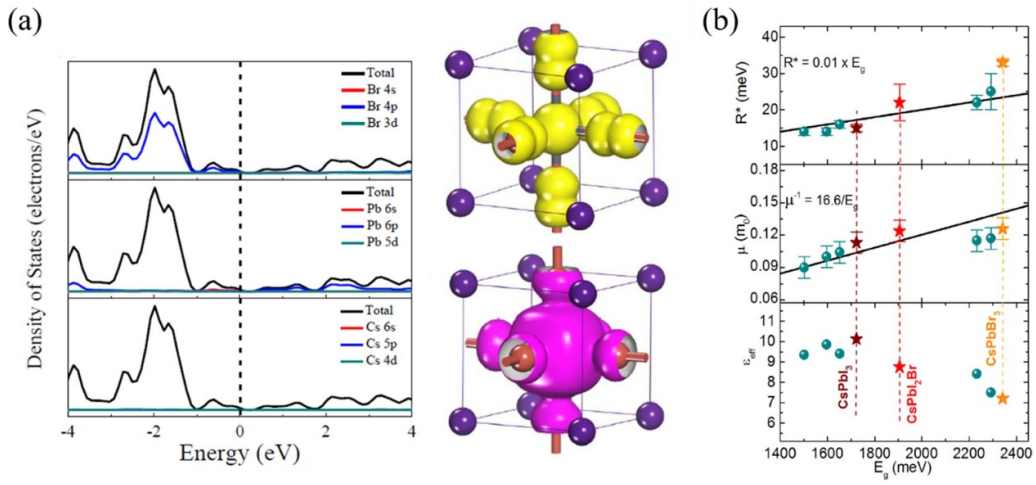

Figure 4. (a) Theoretical calculation results of the electronic structure of cubic $CsPbBr_3$, including the density of states and the corresponding contributions of elements to the energy band, as well as the electronic distribution of the maximum value of the valence band and the minimum value of the conduction band [53]. John Wiley & Sons. [© 2016 WILEY-VCH Verlag GmbH & Co. KGaA, Weinheim]. (b) Binding energy (top), effective mass (middle), and dielectric constant (bottom) versus band gap. Brown, red, and yellow stars represent the results for $CsPbI_3$, $CsPbI_2Br$ and $CsPbBr_3$, respectively. Green spheres indicate another experimental finding. Reprinted with permission from [54]. Copyright (2017) American Chemical Society. CC BY 4.0.

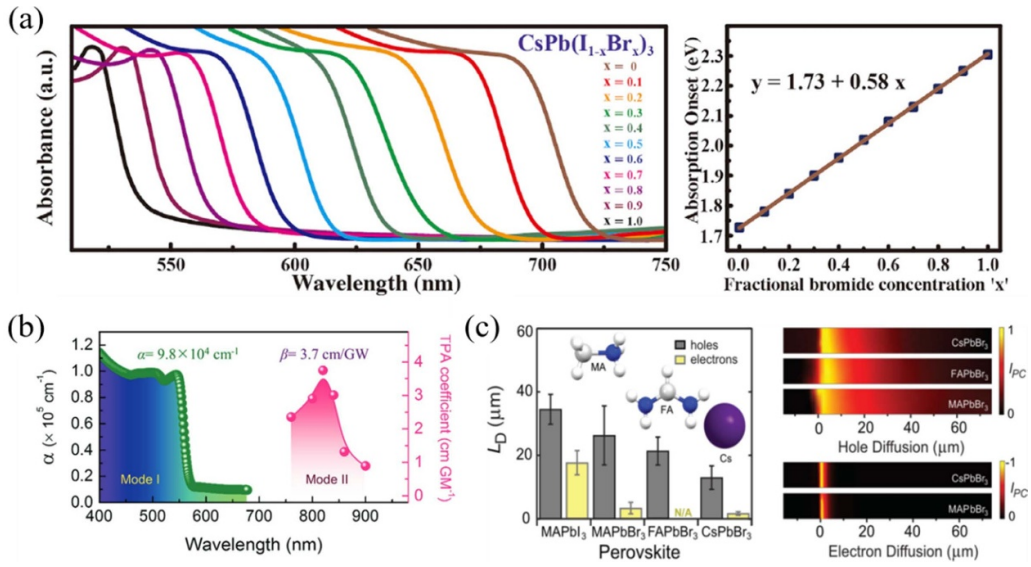

Figure 5. (a) Absorbance spectra for IHP films of different components, $CsPb(I_{1-x}Br_x)_3$. Reprinted from [34], Copyright (2018), with permission from Elsevier. (b) Visible light absorption coefficient and two-photon absorption coefficient of $CsPbBr_3$ single crystal (SC) [57]. John Wiley & Sons. [© 2017 WILEY-VCH Verlag GmbH & Co. KGaA, Weinheim]. (c) The average diffusion lengths measured in $APbBr_3$ SC and previously published $MAPbI_3$ (left), electron and hole diffusion lengths measured in different perovskite components (right). Reprinted with permission from [56]. Copyright (2017) American Chemical Society.

absorption capability of the material as the absorption layer is crucial for highly efficient devices. Generally, the visible light absorption coefficient (α) of the material can be calculated by using the following equation:

$$\alpha = \frac{4\pi k}{\lambda}.$$

Here, the extinction coefficient (k) is determined by ellipsometry [55]. Steele *et al* reported that $CsPbBr_3$ SC wafer has a visible light absorption coefficient of 9.8×10^4 cm^{-1} (figure 5(b)) [52], ten times higher than that of organic dyes, and slightly higher than that of organic–inorganic hybrid perovskites ($MAPbBr_3$ SC). Furthermore, Roy *et al* used scanning photocurrent microscopy and time-resolved microwave conductivity to obtain diffusion lengths of holes and electrons in a series of brominated perovskite-type lead perovskite SCs ($APbBr_3$, $A = MA^+$, FA^+, Cs^+). It was shown that the diffusion length of holes ($L_D^{h^+} \sim 10 - 50\mu m$) was significantly longer than that of electrons ($L_D^{e^-} \sim 1 - 5\mu m$), regardless of the A-type cation. However, the electron diffusion length is

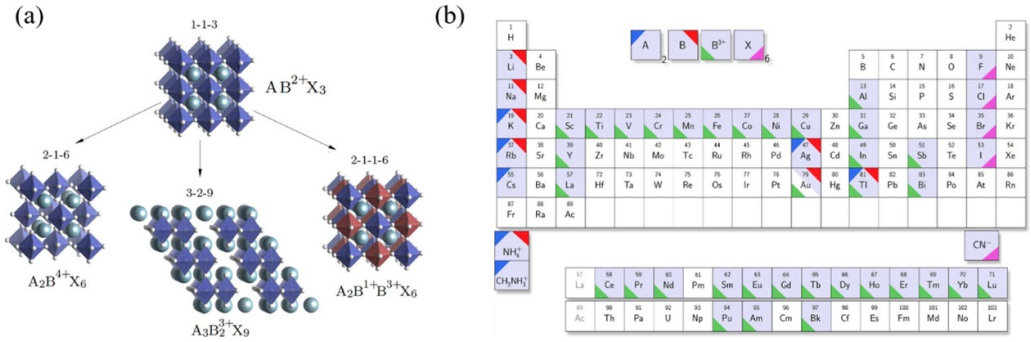

Figure 6. (a) Schematic diagram of the crystal structure relationship between Pb-perovskites and lead-free perovskite derivatives. (b) Elements of halide double perovskites formed by $A_2BB^{3+}X_6$. Reprinted with permission from [63]. Copyright (2016) American Chemical Society.

more significantly affected by the halogen species than the holes (figure 5(c)) [56].

Some lead-free all-inorganic perovskites have also been developed. Among them, the most common is to replace Pb with another group 14 metal (e.g. Sn and Ge) [58–61]. However, the stability of Sn^{2+} and Ge^{2+}-based perovskites in air is not as good as that of Pb^{2+}. They are rapidly oxidized to more stable Sn^{4+} and Ge^{4+} once they are exposed to the air, thus leading to rapid collapse of the 3D perovskite structure. Taking Sn-based perovskite as an example, in order to stabilize the structure, several groups reported Sn-based halide perovskite derivatives with the general composition of Cs_2SnX_6, in which Sn exists in a stable +4 oxidation state with good stability in air and moisture [62]. This $Cs_2Sn_2X_6$ is a cubic double perovskite structure through removing half of the octahedral Sn atoms, which are formed by Cs^+ cation and $[SnI_6]^{2-}$ octahedron as anions, as shown in figure 6(a) [63]. Since Sn vacancy defines the regular sublattice of the double perovskite structure, these compounds are called 'vacancy ordered' double perovskite. This structure shows an abnormally dispersed electronic band structure and direct band gap, and the band gap can be as low as 1.3 eV for Cs_2SnI_6. Non-lead perovskite-type compounds with formula unit $A_3B_2X_9$ (A is monovalent cation, B is trivalent metal cation) are also derived with the concept of 'vacancy ordered perovskite'. In the above structure, one third of the octahedral sites is supposed to be empty in order to maintain charge neutrality. This structure is also known as '2D layered perovskite derivative'. Among them, the most common is to replace Pb^{2+} with Sb^{3+} or Bi^{3+}, for example, $Cs_3Sb_2I_9$ and $Rb_3Sb_2I_8$. Another lead-free perovskite structure is derived from the heterovalent substitution of Pb^{2+} by B site cation pairs with oxidation states of +1 and +3, the so-called 'double perovskite' structure based on bismuth and monovalent metals, for example, $Cs_2AgBiBr_6$ (figure 6(b)) [63]. At present, both theoretically and experimentally, the feasibility of the above alternatives has been confirmed [64, 65].

In the hybrid perovskite photovoltaic community, the facet engineering of perovskite thin films is a new strategy to adjust the film characteristics, such as exquisite control of crystal growth, optoelectronic properties, stability of perovskite materials, types of surface defects and the structure of heterofacets [66, 67]. At present, there are also some aspects of facet engineering being carried out in inorganic perovskite systems. Dong *et al* demonstrated that the preferred (100) of $CsPbBr_3$ SCs and the polar (111) facet have anisotropic surface-dependent electronic structures, defect formation energies and carrier mobilities [68]. Wang *et al* confirmed through experiments and theoretical calculations that β-phase $CsPbI_3$ with a strongly preferred (110) orientation has a lower band gap and is thermodynamically stable compared to the orthogonal α-$CsPbI_3$ and γ-$CsPbI_3$ [41]. Compared with traditional materials, researchers currently pay less attention to facet engineering in inorganic perovskite films. Therefore, there is still considerable room for inorganic perovskite facet engineering to improve device performance.

2.2. Fabrication of IHP films and IHPSCs

As widely accepted today, the PSC is an n–i–p or p–i–n heterojunction solar cell, where the perovskite is used as an intrinsic absorber sandwiched by two selective contacts, i.e. an electron transporting layer (ETL, n) or a hole transporting layer (HTL, p) [61]. Figure 7(a) and table 1 show some representative architectures of PSCs, including regular structure (n–i–p), inverted structure (p–i–n) and HTL-free carbon electrode structure. Much effort have been devoted to improve the performance of IHPSCs, and the efficiency of all these three types of IHPSCs has been rapidly improved in the past few years, as shown in figure 7(b). More recently, Meng *et al* promoted the certificated efficiency of n–i–p-type devices to 20.1% by interface engineering and perovskite passivation, and Liu *et al* fabricated $CsPb(I, Br)_3$-based solar cells with 21.8% efficiency by employing Boc-S-4-methoxy-benzyl-L-cysteine as a passivator to suppress halide vacancies and coordinate with undercoordinated Pb^{2+} [69, 70]. It is worth noting that although the high performance of IHPSCSs so far is basically based on regular structures, some dopants in the HTL used in this structure are detrimental to the stability of the device, which will be discussed in section 4. Compared to the doped organic HTLs, inorganic HTLs, such as NiO, have much less influence on the stability of the inorganic perovskite material and

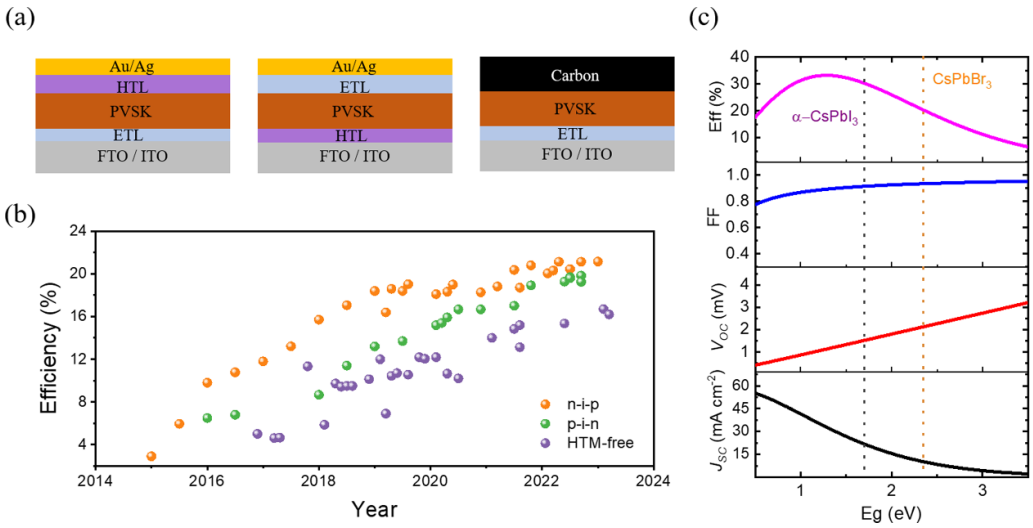

Figure 7. (a) Varieties of device architectures for PSCs. (b) Efficiency evolution of IHPSCs with different architectures [32, 39, 41, 43, 45, 69, 70, 74–77, 79–81]. (c) Relationship between SQ limit of single junction solar cell and band gap of absorber material. (J_{SC}: short circuit current, V_{OC}: open-circuit voltage, FF: fill factor, Eff.: efficiency).

Table 1. Evolution of the device efficiency and stability depending on the components of the absorber material and the device architecture (MPP = maximum power point, RH = relative humidity).

Device architecture	Absorber material	PCE	Stability	References
n–i–p	$CsPbI_3$	21.0%	98% of its initial PCE over 500 h (light intensity = LED illumination (100 mW cm^{-2}), applied bias = 0.85 V, atmosphere = N_2 atmosphere).	[69]
	$CsPbI_{3-x}Br_x$	21.8%	89.3% of its original efficiency at 85 °C for 120 h (atmosphere = N_2 atmosphere).	[70]
p–i–n	$CsPbI_3$	19.84%	95% of its initial efficiency after the same operation for 1000 h (light intensity = LED illumination (100 mW cm^{-2}), applied bias = MPP, atmosphere = N_2 atmosphere, temperature ~45 °C).	[74]
	$CsPbI_{3-x}Br_x$	17.02%	80% of its PCE after 1000 h (light intensity = dark, atmosphere = air atmosphere, RH = 30%).	[79]
HTM-free	$CsPbI_3$	16.7%	80% of their initial PCE at 85 °C for 200 h (atmosphere = air atmosphere, temperature = 20 °C–30 °C, RH = 5%–20%, no encapsulation).	[76]
	$CsPbI_{3-x}Br_x$	14.84%	~94% of its initial PCE after storage for 30 d (atmosphere = air atmosphere, temperature = room temperature, RH = 20%–25%).	[80]
	$CsPbBr_3$	11.08%	Nearly unchanged over 100 d and 85 °C over 30 d (atmosphere = air atmosphere, temperature = 85 °C, RH = 40%, no encapsulation).	[81]

have been successfully used in the inverted structured PSCs [71]. Moreover, this structure is more compatible with the fabrication technology of perovskite-silicon tandem solar cells [72, 73]. Recently, Fu *et al* improved the efficiency of inverted IHPSCs to 19.84% by introducing 1,4-butanediamine to polish the IHP film [74]. IHPSCs based on carbon counter electrodes (C-IHPSCs) has advantages of low-cost fabrication and superior stability because it avoids the use of HTL and precious metal electrodes [75]. To date, the highest efficiency (16.7%) of C-IHPSCs has been reported by Wang *et al* [76]. Although

Table 2. Comparison of different inorganic perovskite deposition methods with their stability and best efficiency documented.

Deposition		Absorber material	PCE	Stability	References
Solution processing	One-step spin-coating	$CsPbI_{3-x}Br_x$	21.8%	89.3% of its original efficiency at 85 °C for 120 h (N_2 atmosphere).	[70]
	Two-step spin-coating	$CsPbI_{3-x}Br_x$	12.5%	98% of the initial PCE for 480 h (stored under ambient conditions without encapsulation).	[87]
Vacuum deposition processing		$CsPbI_2Br$	11.8%	Stabilized PCE of 11.5% (stored in the dark with encapsulations).	[88]

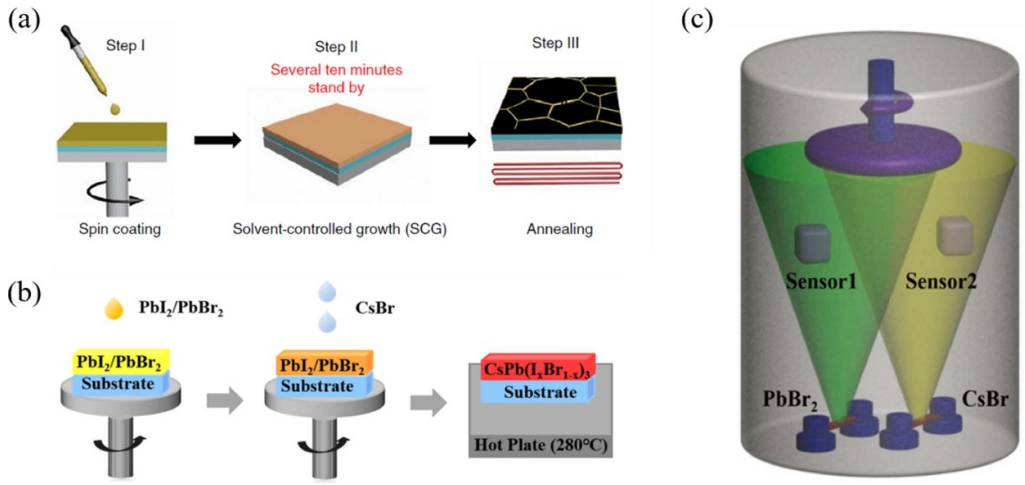

Figure 8. Illustration of preparing IHP absorption layers by different methods. (a) One-step deposition. Reproduced from [39], with permission from Springer Nature. CC BY 4.0. (b) Multi-step deposition. Reproduced with permission from [87]. Copyright 2018, the Royal Society of Chemistry. (c) Vacuum deposition [90]. John Wiley & Sons. [© 2018 WILEY-VCH Verlag GmbH & Co. KGaA, Weinheim].

the efficiency of the IHPSCs has achieved these exciting results, the reported efficiencies are still far below the SQ theoretical limit, as shown in figure 7(c) [77, 78].

Regarding the fabrication methods of the IHPSCs, the preparation of IHPs with high crystalline quality is a prerequisite for high device performance (table 2) [70, 77, 82–88]. Solution processing methods, such as spin coating, is the most widely used approach for IHPs. For the one-step spin coating method, the $CsPbX_3$ precursor is first dissolved in a suitable solvent with a certain stoichiometric ratio, then spin-coated, and finally annealed, as shown in figure 8(a) [39]. Common solvents are dimethylformamide (DMF), dimethyl sulfoxide (DMSO) or a mixture of the two. During the spin coating process, anti-solvent (ATS), such as chlorobenzene, benzene, xylene, toluene, isopropanol (IPA), ethyl acetate and chloroform, can be used to increase the nucleation rate of the precursor solution and thus to improve the morphology and coverage of the film [86]. Compared to hybrid perovskites, the crystallization of IHPs usually requires a higher annealing temperature. Although this one-step method is relatively simple, it is difficult to control the film quality and repeatability of IHPs. Subsequent research found that high-quality absorber films can be obtained by solvent-controlled growth.

Nonetheless, the one-step method is not suitable for $CsPb(I, Br)_3$ with a high proportion of Br due to the solubility limit of Cs salts, especially CsBr (ca. 0.25 M in DMSO, ca. 0.5 M together with $PbBr_2$) [87, 89]. In particular, one thing that has to be addressed is that the performance enhancement of the IHPSCs is attributed to the replacement of PbI_2 with $DMAPbI_3$ for the one-step spin coating method [44]. As shown in figure 8(b), the two-step method involves a deposition of the PbX_2 layer and then a reaction between PbX_2 and CsX via a multi-step dip coating or spin coating process. Further annealing affords the desired crystal phase. This method is usually used to fabricate $CsPbBr_3$ and $CsPbIBr_2$ films because it can overcome the solubility limit in the one-step method.

The IHPs can also be deposited by a vacuum vapor method, such as a dual-source thermal evaporation, as depicted in figure 8(c) [90]. Using the vacuum deposition method, the thickness and composition of the resulting film can be precisely controlled as well as the high repeatability. Hutter *et al* used time-resolved microwave conductivity technology to study the photoelectric properties of vapor-deposited and spin-coated black-phase $CsPbI_3$ thin films [91]. The results showed that the carrier lifetime of vapor-deposited $CsPbI_3$ unexpectedly exceeded 10 μs, whereas the carrier lifetime of the spin-coated samples was only 0.2 μs. Therefore, the device corresponding to the $CsPbI_3$ films based on vapor deposition has higher efficiency than that based on the solution method. Chen *et al* prepared high-quality $CsPbBr_3$ films by this method and used it for the inorganic-perovskite/organic four-terminal tandem solar cell, obtaining an efficiency of 14.03%, which is the highest efficiency of this structure [90].

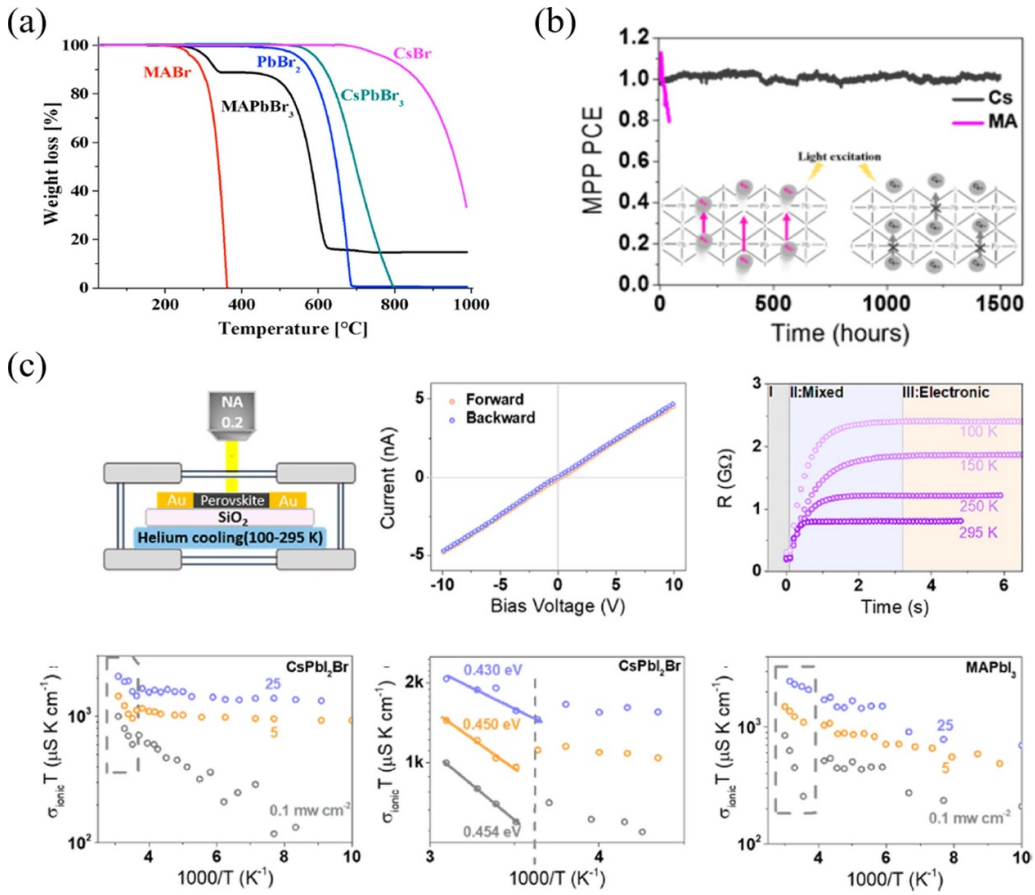

Figure 9. (a) TGA of MABr, $PbBr_2$, CsBr, $MAPbBr_3$ and $CsPbBr_3$. Reprinted with permission from [93]. Copyright (2016) American Chemical Society. (b) MPP test of the unsealed $CsPbI_2Br$ (dark gray line) and $MAPbI_3$ solar cells (magenta line) in a nitrogen glovebox (25 °C). Reprinted with permission from [38]. Copyright (2017) American Chemical Society. (c) Ionic conductivity of $CsPbI_2Br$ and $MAPbI_3$ film in Au/perovskite/Au lateral structures by cryogenic galvanostatic and current−voltage experiments. Reprinted with permission from [38]. Copyright (2017) American Chemical Society.

3. Stability of IHPs

3.1. Thermal and light stabilities

The unsatisfactory thermal stability of the organic–inorganic hybrid perovskite comes from its volatile organic cations, such as FA^+ and MA^+, which are easily lost at moderate temperature (i.e. 100 °C), eventually leading to the thermal decomposition of the perovskite [17, 92]. These problems can be easily solved by replacing the organic cations FA^+ and MA^+ with the inorganic cation Cs^+. Cache *et al* explained the difference in thermal stability between $MAPbBr_3$ and $CsPbBr_3$ by thermogravimetric analyses (TGA) and confirmed that $CsPbBr_3$ (weight loss onset ∼570 °C) has much better thermal stability than $MAPbBr_3$ (weight loss onset ∼220 °C), as shown in figure 9(a) [93]. Moreover, the IHPs exhibit much better operational stabilities under continuous light illumination and electrical biases. Zhao *et al* demonstrated that the IHPSC based on $CsPb(I, Br)_3$ can sustain its initial efficiency even after 1500 h maximum power point (MPP) operation (figure 9(b)) [38]. Much better operational stability was found to arise from the suppressed ion migration in the IHPs. $CsPb(I, Br)_3$ was measured to have an ion migration activation energy of ∼0.45 eV, almost independent of the light illumination. Comparatively, the ion migration activation energy of the hybrid perovskite was significantly reduced under a weak light, as shown in figure 9(c) [38]. This difference in the light illumination-dependent ion migration behavior may come from the different rotation freedoms of A-site cations. The much lower rotation freedom of Cs should be able to help stabilize the lattice structure when under light-induced complicated electron–lattice and light–matter interactions.

3.2. Phase stability

Currently, to the best of our knowledge, the IHPSCs with the highest efficiency are based on $CsPbI_3$. $CsPbI_3$ has a relatively narrower band gap compared to that of $CsPb(I, Br)_2$, much better material stability compared to $CsSn(I. Br)_3$ and more mature preparation technology. However, a relatively low tolerance factor of 0.807 makes black-phase $CsPbI_3$ thermodynamically unstable at room temperature. A feasible way is to substitute an appropriate number of I^- ions with smaller size Br^- ions or Cl^- ions. Sutton *et al* have for the first time reported enhanced ambient stability of

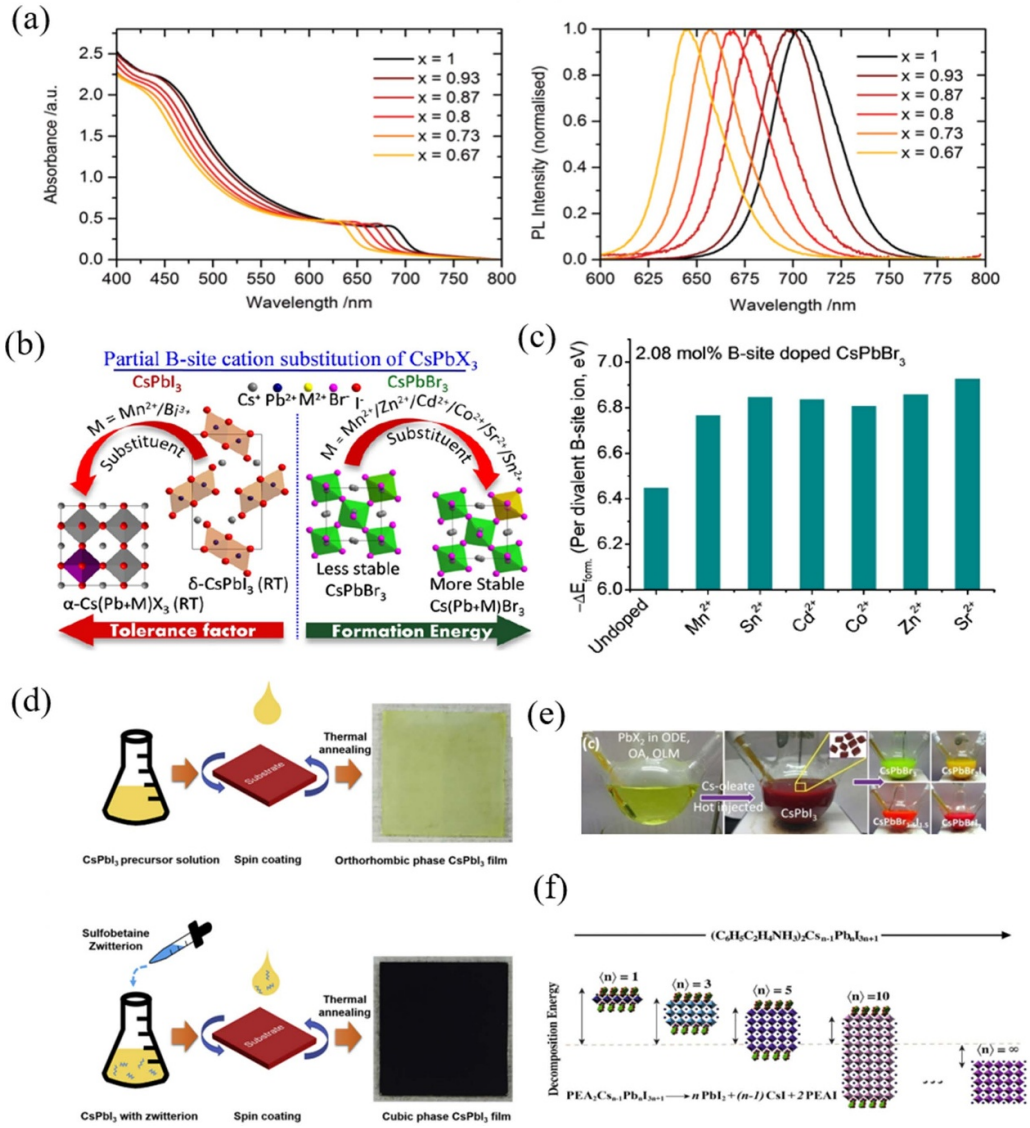

Figure 10. (a) Absorbance spectra and photoluminescence spectra for $CsPb(I_xBr_{1-x})_3$ films with varying iodide concentration 'x'. [36] John Wiley & Sons. [© 2016 WILEY-VCH Verlag GmbH & Co. KGaA, Weinheim]. (b) Schematic diagram of Pb^{2+} partially replaced by various metal ions (doping or alloying) can improve the stability of α-$CsPbI_3$ at room temperature by increasing the tolerance factor, and improve the thermal stability of orthogonal $CsPbBr_3$ by increasing the formation energy. Reprinted with permission from [100]. Copyright (2018) American Chemical Society. (c) Histograms comparing the first-principles calculation results of the formation energy (ΔE_{form}) changes of each divalent Pb^{2+} ion in $CsPbBr_3$ nanocrystals when undoped and doped with 2.08 mol% of various metal ions. Reprinted with permission from [100]. Copyright (2018) American Chemical Society. Schematic diagram of reducing grain size (d) nanocrystal. Reprinted from [101], Copyright (2017), with permission from Elsevier. (e) Quantum dots (QDs). Reprinted from [102], Copyright (2018), with permission from Elsevier. (f) 2D perovskite. Reprinted from [34], Copyright (2018), with permission from Elsevier.

bandgap-tunable $CsPb(I_xBr_{1-x})_3$ (figure 10(a)) compared to $CsPbI_3$ [36]. Tian *et al* prepared the IHP films through composition engineering, and the resulting solar cells gained a remarkable long-term operational stability [94]. However, this anion alloying method extends the band gap of the material and narrows the absorption range [34]. At the same time, under light or electron beams, phase segregation may occur when Br^- ions are introduced into IHP films [95]. Fortunately, theoretical calculations reported by Yin *et al* showed that $CsPbI_2Br$ has a stable alloy phase that results from strong Coulomb interactions in the ionic perovskite lattice [96]. Some relatively stable $CsPbI_2Br$ perovskites have been reported in experiments [97–99].

As mentioned above, partial substitution of I^- with Br^- induces an increased band gap, which has a negative impact on the efficiency of solar cells. From different perspectives, experimental and theoretical calculation results have shown that B-site doping/alloying strategies have no obvious influence on the band gap of the perovskite material, and can improve the phase stability of IHPs as well. A variety of less toxic inorganic cations, such as Sn^{2+}, Ge^{2+}, Co^{2+}, Mn^{2+}, Bi^{3+}, Eu^{3+} and Nb^{5+} have been employed to partially

replace B-site ions to tune the tolerance factor or the formation energy, as shown in figure 10(b) [100]. An increase in the formation energy of B-site doped $CsPbBr_3$ suggests an enhancement of the thermodynamic stability of orthorhombic $CsPbBr_3$ (figure 10(c)) [100]. Eco-friendly Sn^{2+}, which has a slightly smaller size than Pb^{2+}, exhibits a potential in adjusting the tolerance factor, thus achieving higher phase stability. However, $CsSnI_3$ has proved to be unstable under ambient conditions due to the oxidation of Sn^{2+} to Sn^{4+} within IHP films. Stabilizing the valence state of Sn^{2+} in Sn-based IHPs is also the focus of the study of the stability of IHPs. Li *et al* obtained $CsSnIBr_2$ thin films with low Sn vacancy by using hypophosphorous acid (HPA) additive. With the assistance of HPA, the formation of Sn^{4+} was inhibited in the preparation process of $CsSnIBr_2$ thin films, thus resulting in superior thermal stability [103]. Germanium (Ge) is recognized as a suitable B-site dopant against phase instability, and a full-coverage native-oxide layer can be formed while using Ge doping [104, 105]. In addition, aliovalent B-site doped with Bi^{3+}, Eu^{3+}, Nb^{5+}, etc, is also used to enhance the phase stability of IHPs [106–108].

Earlier studies have shown that the phase stability of IHPs is grain size-dependent; the phase stability can be improved with decreasing grain sizes [101]. As shown in figure 10(d), Huang *et al* found that mixing a small number of sulfobetaine zwitterions in the $CsPbI_3$ precursor solution can stabilize the α phase of the $CsPbI_3$ films at room temperature. The interaction between zwitterions and $CsPbI_3$ hinders the rapid crystallization of $CsPbI_3$, which reduces the grain size of $CsPbI_3$, thus stabilizing the α phase. On the other hand, it has been reported that α-$CsPbI_3$ QDs and nanocrystals ranging in size from 4–15 nm are phase-stable for months in ambient air, whereas α-$CsPbI_3$ nanocrystals ranging in size from 100–200 nm quickly transform from the black phase to the non-perovskite phase. This stability seems to be related to crystal size rather than having an apparent connection with size effects. Thus, in more cases, the most perovskite QDs 10–30 nm in size were reported to be more appropriate as nanocrystals. The dependence of the halide composition on the stability of IHPSCs has also been studied in detail (figure 10(e)) [102]. It is revealed that, as mentioned above, Br doping for $CsPbI_3$ strongly enhances the stability of the resulting IHP QDs under ambient atmosphere. Furthermore, it is demonstrated that quasi-2D perovskites (figure 10(f)), induced by a judicious amount of phenylethyl ammonium iodide, can remarkably suppress undesirable phase transition [34]. Recently, a 2D–3D all-inorganic $Cs_2PbI_2Cl_2$–$CsPbI_{2.5}Br_{0.5}$ perovskite was successfully developed to address the phase instability issue of IHPs [109].

In addition to the common strategies described above, some other effective methods have also been developed to improve the phase stability of IHPs. Li and co-workers reported poly-vinylpyrrolidone (PVP)-induced surface passivation engineering to stabilize cubic-phase $CsPbI_3$ [110]. Acylamino groups of PVP induced electron cloud density enhancement on the $CsPbI_3$ surface and reduced the surface energy, which is conducive to stabilize α-$CsPbI_3$. Xu *et al* introduced an ultrathin 2D perovskite on the top of 3D IHPs through the self-assembly method [99]. Ultrathin 2D perovskite can prevent moisture penetration, thus improving the stability of IHPs.

4. Stability of inorganic PSCs

In this section, we summarize several methods to improve the stability of IHPSCs, such as optimization of bulk materials, charge transport layer, interface engineering, carbon counter electrode and device encapsulations.

4.1. Optimization of bulk materials

There is no doubt that improving the crystal quality of IHP is the most effective way to enhance the device stability. Chen *et al* controlled the α-$CsPbI_2Br$ crystal growth by a gradient thermal annealing (GTA) method and further optimized the film morphology by using green ATS IPA (figure 11(a)) [86]. By using this GTA-ATS synergistic effect, high-quality perovskite thin films were obtained and as a result, the corresponding devices exhibited excellent moisture and oxygen resistance ability. As shown in figure 11(b), Zhao *et al* fabricated orthorhombic γ-$CsPbI_3$ thin film with inherent thermodynamic stability through a simple solution process, and manipulated the formation of a size-dependent phase through a proton transfer reaction by using a small amount of H_2O [111]. Further theoretical calculation results show that γ-$CsPbI_3$ with lower surface free energy has better thermodynamic stability than δ-$CsPbI_3$when its surface area is greater than 8600 $m^2\ mol^{-1}$ and has equivalent photoelectric performance to α-$CsPbI_3$. It has also proved effective by adding an appropriate amount of molten salt additives to the all-inorganic perovskite precursor solution to assist the crystallization of the absorption layer [42, 112]. Yu *et al* developed a urea-ammonium thiocyanate molten salt modification strategy to fully release and exploit the coordination activities of SCN^- to deposit high-quality $CsPbI_3$ film for efficient and stable all-inorganic solar cells (figure 11(c)) [42]. Zhang *et al* proposed the use of lead formate ($C_2H_2O_4Pb$) as molten salt to control the crystallization process. The introduction of this molten salt can not only accelerate the mass transfer process, but also reduce the formation barrier energy that changes the crystallization path, thus forming a high-quality perovskite film that can inhibit the formation of pinholes and cracks (figure 11(d)) [112]. Recently, Cui *et al* developed a new precursor solution system based on a new room-temperature molten salt as a solvent, dimethylamine acetate (DMAAc), to improve the crystallinity of $CsPbI_3$ perovskite (figure 11(d)) [46]. In addition, these methods to improve the phase stability of IHPs are also beneficial to the device stability.

4.2. Interfacial engineering

The properties of the active layer are surely important to the cell performance of IHPSCs, but by the same token device

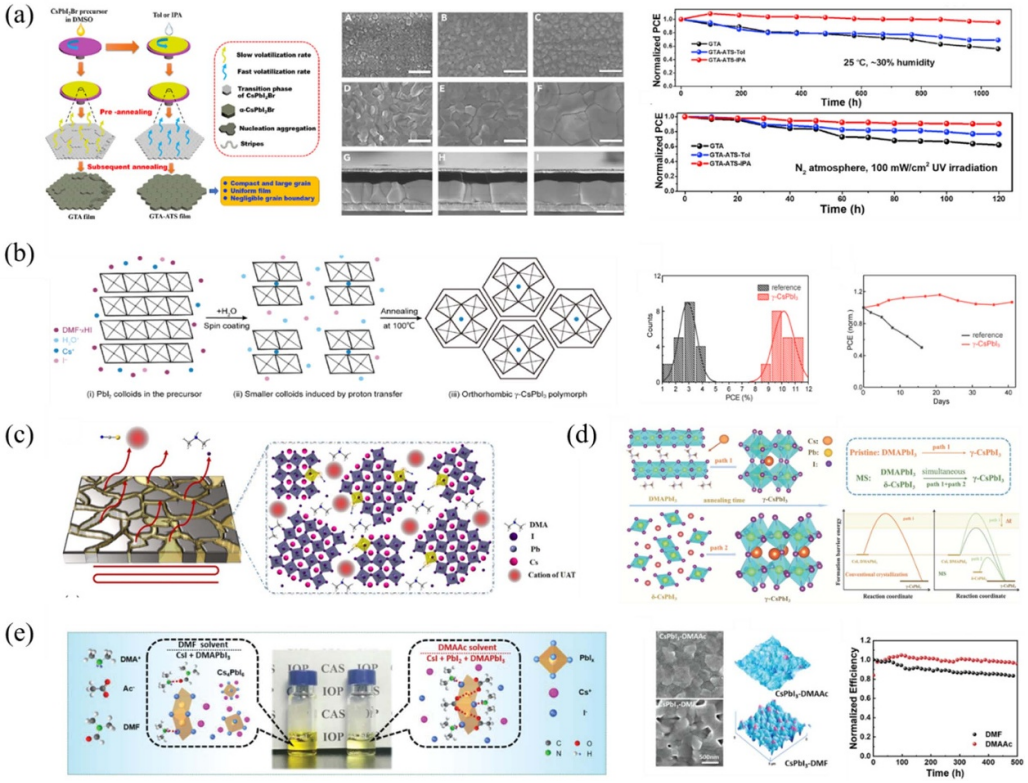

Figure 11. (a) Schematic diagram of the crystallization process of $CsPbI_2Br$ perovskite treated with GTA or GTA-ATS; SEM images of corresponding films and stability characterization of the corresponding device. Reprinted from [86], Copyright (2019), with permission from Elsevier. (b) Schematic diagram of the stabilization of γ-phase $CsPbI_3$, the histogram of the PCE values corresponding to devices with different crystal phase absorption layers and their stability as a function of storage time. Reprinted with permission from [111]. Copyright (2018) American Chemical Society. (c) Scheme for the perovskite crystal growth and additive volatilization of the film [42]. John Wiley & Sons. [© 2021 WILEY-VCH Verlag GmbH & Co. KGaA, Weinheim]. (d) Schematic phase conversion and mechanism for the accelerated crystallization process based on the pristine and molten-salt-assisted crystallization films [112]. John Wiley & Sons. [© 2021 WILEY-VCH Verlag GmbH & Co. KGaA, Weinheim]. (e) Photographs of perovskite precursor solutions based on DMAAc and DMF solvents, schematic diagrams of cation/anion/solvent interactions in the solutions and the stability characterization of the corresponding device [46]. John Wiley & Sons. [© 2022 WILEY-VCH Verlag GmbH & Co. KGaA, Weinheim].

interfaces cannot be ignored. In recent years, remarkable advancements in IHPSCs have been realized through efficient interface engineering using different interface materials including some halogen salts between charge transport and absorption layers. Interfacial treatment can be realized by vacuum or solution methods, which is one of the main topics of interest for academic and industrial researchers.

Similar to organic–inorganic halide PSCs, IHPSCs also use SnO_2, TiO_2, C_{60}, ZnO, etc, as ETLs, especially the most widely used TiO_2 and SnO_2 [39, 69, 113]. Previous studies have shown that SnO_2 has a lower conduction band and higher electron mobility compared to TiO_2, therefore attracting more attention recently [114, 115]. In earlier studies, it was found that the conduction band position of SnO_2 may not perfectly match that of IHPs. Ye *et al* found that lithium fluoride (LiF) treatment on the ETL SnO_2 can present better energy level alignment in the device and passivate interface defects as well (figure 12(a)) [116]. Further optimization can also bring better device performance with high light stability and high efficiency (>18%).

As mentioned in section 2.2, choosing suitable HTLs is also the key to fabricate high-performance IHPSCs. Suitable HTLs need to meet several requirements, including high mobility, optimal highest occupied molecular orbital energy level, good solubility and film forming properties and low cost. In earlier studies, HTLs were usually doped to improve their hole mobility, for example, spiro-OMeTAD doped with bis(trifluoromethane)sulfonimide lithium salt (Li-TFSI) [117]. However, severe degradation was reported for IHPSCs due to the existence of dopants (e.g. 4-tert-butyl pyridine and lithium salts) [118, 119]. Therefore, some research groups attempted a variety of valuable works, such as using hydrophobic HTL and introducing a hydrophobic layer at the conventional IHPs/HTL interface. As shown in figure 12(b), Tan *et al* found that the treatment towards $CsPbI_3$ with phenyltrimethylammonium iodide (PTAI) could significantly improve the phase stability of IHP and the device stability, but would not cause the change in the band gap of light absorber [69]. This positive effect is attributed to the formation of PTAI-based low-dimensional perovskite distributed at the grain

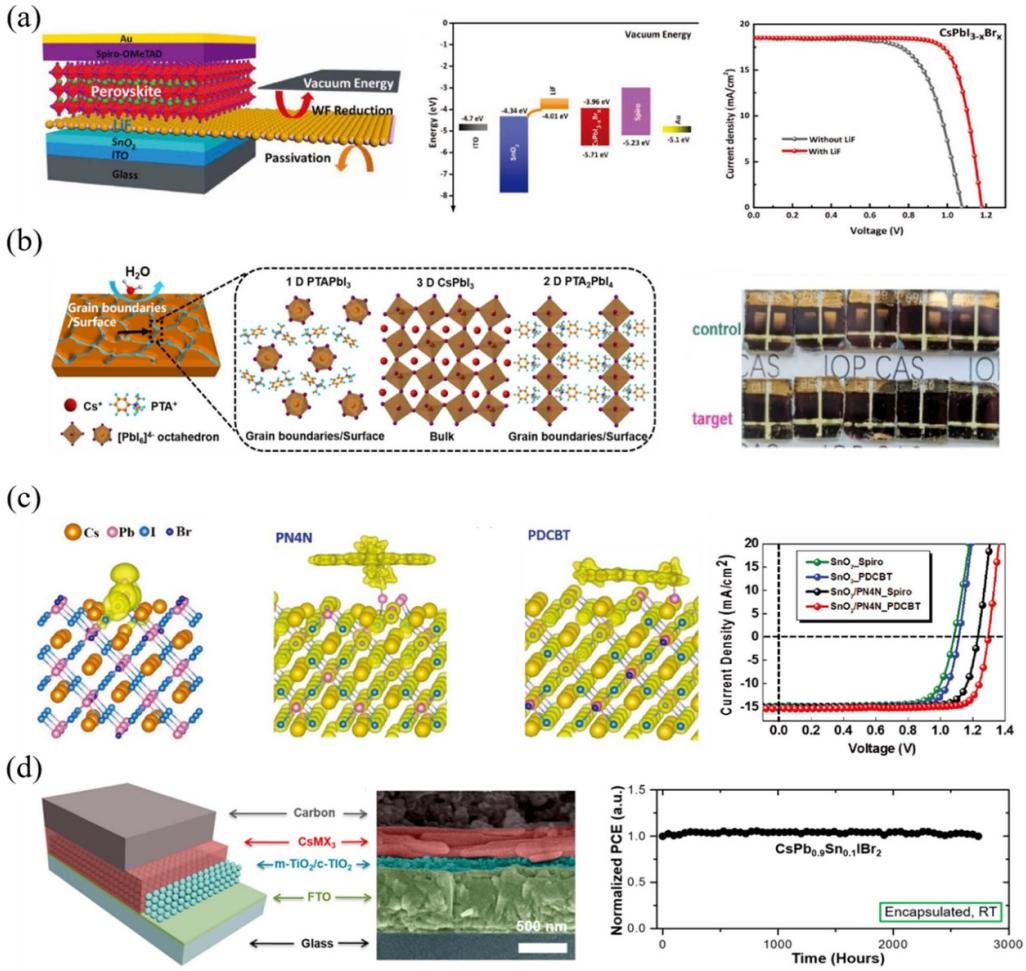

Figure 12. (a) ETL/IHP interface modified by LiF [116]. John Wiley & Sons. [© 2019 WILEY-VCH Verlag GmbH & Co. KGaA, Weinheim]. (b) Schematic diagram of 3D $CsPbI_3$ treated with 1D $PTAPbI_3$ and 2D PTA_2PbI_4 composition at the grain boundaries, and long-term stability testing of unencapsulated devices under ambient conditions [69]. John Wiley & Sons. [© 2022 WILEY-VCH Verlag GmbH & Co. KGaA, Weinheim]. (c) Simultaneous modification of ETL/PVSK and PVSK/HTL interfaces [96]. John Wiley & Sons. [© 2019 WILEY-VCH Verlag GmbH & Co. KGaA, Weinheim]. (d) $CsMX_3$ perovskite solar cells based on carbon electrode instead of gold electrode. Reprinted with permission from [120]. Copyright (2017) American Chemical Society.

boundaries, which not only enhances the phase stability of $CsPbI_3$, but also effectively suppresses non-radiative recombination. These results show that the treatment towards the back surface of IHPs with organic halides containing hydrophobic functional groups can improve both the efficiency and stability of the device. Tian *et al* used an amino-functionalized polymer PN4N as the interface modification layer and an undoped polymer PDCBT as the HTL for $CsPb(I, Br)_3$-based solar cells (figure 12(c)) [96]. The introduction of these two layers can realize high-quality perovskite films with better energy level matching and strong electronic interactions, thus resulting in double interface synergistic passivation of surface defects. In addition, the employment of carbon counter electrodes and encapsulation technology have greatly improved the device stability, as shown in figure 12(d) [120].

In order to obtain highly stable IHPSCs, it is necessary to integrate more passivation methods, such as low-dimensional interface materials, undoped HTLs and encapsulation technologies. Heo *et al* modified $CsPbI_3$ perovskite films with oxidized MXene (OMXene) nanoplates based on orthogonal spray coating [121]. This method not only improves the humidity stability of the absorption layer, but also enhances the charge separation at the perovskite/ETL interface. Finally, the PSC module based on this method has good hygrothermal and photoelectric stability, as shown in figure 13(a). Recently, Zhao *et al* reported more exciting results on the stability of IHPSCs (figure 13(b)) [109]. This work introduced a 2D $Cs_2PbI_2Cl_2$ coating between the perovskite active layer and the HTL to stabilize the interface and carry out the accelerated degradation of encapsulated IHPSCs under constant light and elevated temperature up to 110 °C. According to the results, it was predicted that the inherent life of the device based on this structure under continuous operation at 35 °C could be 51 000 ± 7000 h (>5 years).

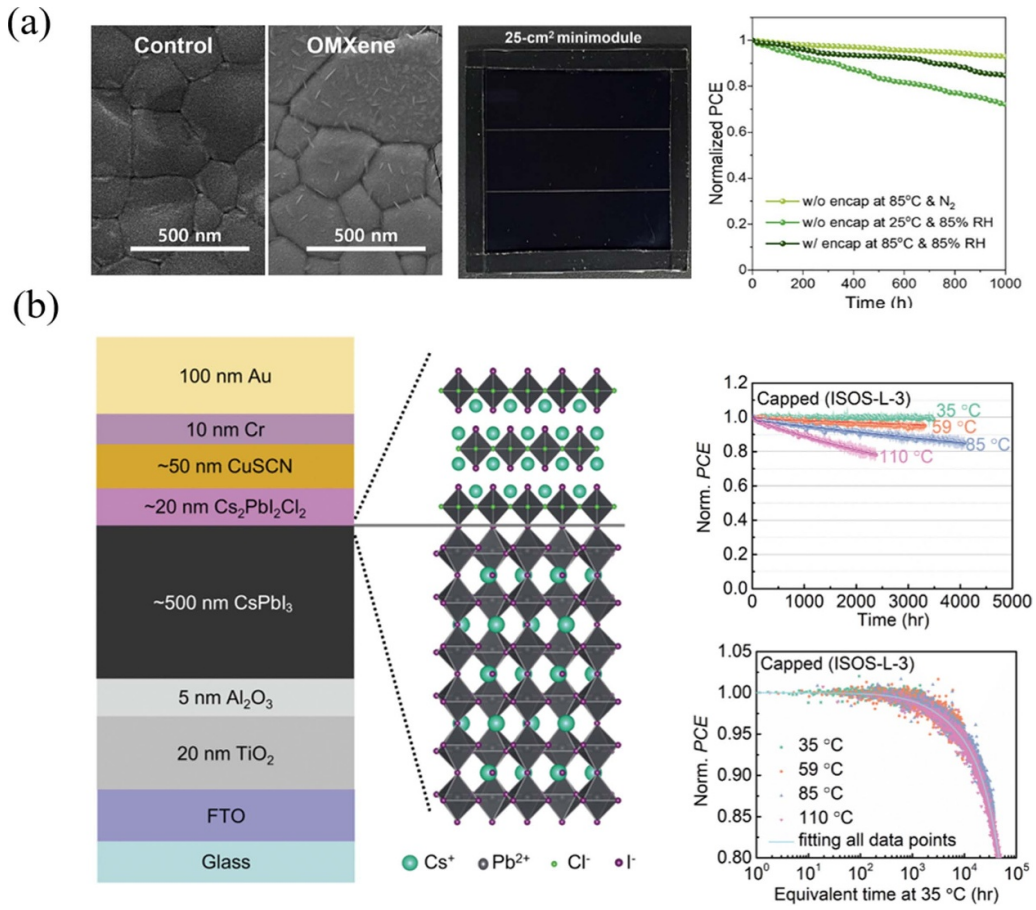

Figure 13. (a) SEM surface images of the $CsPbI_3$ perovskite films, the photographs of a $CsPbI_3$ perovskite minimodule and long-term stability test of an encapsulated $CsPbI_3$ perovskite minimodule under different conditions. Reprinted from [121], Copyright (2022), with permission from Elsevier. (b) Schematic diagram of the device structure with a 2D $Cs_2PbI_2Cl_2$ layer at the top of the 3D perovskite active layer (left). Accelerated aging of PSCs operating at elevated temperatures (right). Reprinted from [109], with permission from AAAS.

5. Future perspectives

In summary, IHPSCs have become a research hotspot due to their superior thermal stability and light stability, especially, their suitable top cells for tandem solar cells. Currently, the serious phase instability issue of the IHP, especially for $CsPbI_3$, has hampered further development of IHPSCs. In response to this problem, many works have proposed their own solutions, which are divided into the following categories:

(1) Self-optimization of IHPs including solvent engineering, halogen site replacement, B doping and alloying, and reducing particle size and dimensions. There is no doubt that the stability of IHPSC mainly depends on the properties of the active layer. By regulating the nucleation and crystallization process of the fully inorganic perovskite absorption layer, a thermodynamically stable phase structure is obtained.

(2) Interface optimization including the selection of ETL and HTL materials, introducing a passivation layer at the ETL/perovskite and HTL/perovskite interface. In this section, on the one hand, it is necessary to consider the arrangement of energy bands between each layer; on the other hand, the *in situ* generation of 2D phases can also suppress the phase transition of the absorption layer at high humidity. In addition, compared to ETL, HTL has a greater impact on the stability of IHPSCs. However, previous studies have shown that devices without HTL layers can significantly improve device efficiency, which still lags behind devices with HTL. At present, some inorganic materials, such as metal oxides, carbon derivatives (carbon, graphene or carbon nanotubes) or other organic materials have been successfully introduced as substitutes for spiro-OMeTAD and have expanded their stability in some cases.

(3) The employment of carbon electrodes and encapsulation technology. Carbon electrodes have much better thermal stability compared to metal electrodes, so combining carbon electrodes with fully IHP absorption layers is more conducive to thermally stable devices. In addition, it is necessary to develop an internal and external packaging strategy for IHPSCs, which are sensitive to humidity. Internal packaging can be achieved by introducing interfacial hydrophobic layers, while external packaging can be achieved using insulating encapsulation films that are widely used commercially.

The stabilities of IHPs and IHPSCs are often closely related to their defect properties, especially due to the more complex formation process of IHPs and the significant lattice distortion caused by competition. In addition to the top surface, we also need to pay more attention to the passivation effect of bulk perovskite and bottom surface defects. We also need to explore more interface materials that can withstand high temperatures to buffer the rigid contact, lattice mismatch, and interface stress between the inorganic charge transfer layer substrate and IHPs.

Although IHPSCs have made exciting progress in stability and efficiency, there is still much more room for improvement in the following aspects. First, from a certain perspective, currently most of all inorganic perovskite materials are more sensitive to humidity than hybrid calcium titanium materials, and they are in metastable phases at room temperature. Therefore, there is still a long way to go to improve the phase stability of all inorganic perovskite materials. Second, how to combine IHPSCs with silicon solar cells to fabricate high-performance tandem photovoltaic devices is a research hotspot in the future. Third, we should find new ways to prepare more efficient and stable devices in the future with the aid of theoretical calculations and some more photophysical methods. Finally, the manufacturing technology, as well as the modification of device structures and materials, has to comply with the ease of large-scale IHPSC manufacturing.

Acknowledgments

We gratefully acknowledge the financial support from the National Natural Science Foundation of China (Grant Nos. 52203368, 52102332, 52072402, 52172260, 52227803 and 52222212), the Ministry of Science and Technology of the People's Republic of China (Grant Nos. 2021YFB3800103 and 2021YFB3800105), the Beijing Natural Science Foundation (Grant No. 2222082) and the CAS-CSIRO Joint Project (Grant No. 112111KYSB20210017).

ORCID iD

Qingbo Meng https://orcid.org/0000-0003-4531-4700

References

[1] Sun S, Salim T, Mathews N, Duchamp M, Boothroyd C, Xing G, Sum T C and Lam Y M 2014 The origin of high efficiency in low-temperature solution-processable bilayer organometal halide hybrid solar cells *Energy Environ. Sci.* **7** 399–407

[2] Stranks S D, Eperon G E, Grancini G, Menelaou C, Alcocer M J, Leijtens T, Herz L M, Petrozza A and Snaith H J 2013 Electron-hole diffusion lengths exceeding 1 micrometer in an organometal trihalide perovskite absorber *Science* **342** 341–4

[3] Ponseca C S *et al* 2014 Organometal halide perovskite solar cell materials rationalized: ultrafast charge generation, high and microsecond-long balanced mobilities, and slow recombination *J. Am. Chem. Soc.* **136** 5189–92

[4] D'Innocenzo V, Grancini G, Alcocer M J, Kandada A R, Stranks S D, Lee M M, Lanzani G, Snaith H J and Petrozza A 2014 Excitons versus free charges in organo-lead tri-halide perovskites *Nat. Commun.* **5** 3586

[5] NREL 2023 Best research-cell efficiency chart: NREL (available at: www.nrel.gov/pv/cell-efficiency.html) (Accessed 1 December 2023)

[6] Kojima A, Teshima K, Shirai Y and Miyasaka T 2009 Organometal halide perovskites as visible-light sensitizers for photovoltaic cells *J. Am. Chem. Soc.* **131** 6050–1

[7] Kim H-S *et al* 2012 Lead iodide perovskite sensitized all-solid-state submicron thin film mesoscopic solar cell with efficiency exceeding 9% *Sci. Rep.* **2** 591

[8] Lee M M, Teuscher J, Miyasaka T, Murakami T N and Snaith H J 2012 Efficient hybrid solar cells based on meso-superstructured organometal halide perovskites *Science* **338** 643–7

[9] Burschka J, Pellet N, Moon S J, Humphry-Baker R, Gao P, Nazeeruddin M K and Gratzel M 2013 Sequential deposition as a route to high-performance perovskite-sensitized solar cells *Nature* **499** 316–9

[10] Jeon N J, Noh J H, Yang W S, Kim Y C, Ryu S, Seo J and Seok S I 2015 Compositional engineering of perovskite materials for high-performance solar cells *Nature* **517** 476–80

[11] Yang W S, Noh J H, Jeon N J, Kim Y C, Ryu S, Seo J and Seok S I 2015 High-performance photovoltaic perovskite layers fabricated through intramolecular exchange *Science* **348** 1234–7

[12] Zhao Y *et al* 2022 Inactive $(PbI_2)_2RbCl$ stabilizes perovskite films for efficient solar cells *Science* **377** 531–4

[13] Park J, Kim J, Yun H-S, Paik M J, Noh E, Mun H J, Kim M G, Shin T J and Seok S I 2023 Controlled growth of perovskite layers with volatile alkylammonium chlorides *Nature* **616** 724–30

[14] Green M A, Ho-Baillie A and Snaith H J 2014 The emergence of perovskite solar cells *Nat. Photon.* **8** 506–14

[15] Frost J M, Butler K T, Brivio F, Hendon C H, van Schilfgaarde M and Walsh A 2014 Atomistic origins of high-performance in hybrid halide perovskite solar cells *Nano Lett.* **14** 2584–90

[16] Boyd C C, Cheacharoen R, Leijtens T and McGehee M D 2019 Understanding degradation mechanisms and improving stability of perovskite photovoltaics *Chem. Rev.* **119** 3418–51

[17] Turren-Cruz S H, Hagfeldt A and Saliba M 2018 Methylammonium-free, high-performance, and stable perovskite solar cells on a planar architecture *Science* **362** 449–53

[18] Yang Y and You J 2017 Make perovskite solar cells stable *Nature* **5** 155–6

[19] Kim M *et al* 2019 Methylammonium chloride induces intermediate phase stabilization for efficient perovskite solar cells *Joule* **3** 2179–92

[20] Bu T *et al* 2022 Modulating crystal growth of formamidinium–caesium perovskites for over 200 cm^2 photovoltaic sub-modules *Nat. Energy* **7** 528–36

[21] Jiang Q, Zhao Y, Zhang X, Yang X, Chen Y, Chu Z, Ye Q F, Li X, Yin Z and You J 2019 Surface passivation of perovskite film for efficient solar cells *Nat. Photon.* **13** 460–6

[22] Wu G, Liang R, Ge M, Sun G, Zhang Y and Xing G 2022 Surface passivation using 2D perovskites toward efficient and stable perovskite solar cells *Adv. Mater.* **34** e2105635

[23] Zhou N, Shen Y, Li L, Tan S, Liu N, Zheng G, Chen Q and Zhou H 2018 Exploration of crystallization kinetics in quasi two-dimensional perovskite and high performance solar cells *J. Am. Chem. Soc.* **140** 459–65

[24] Wang T *et al* 2022 Transporting holes stably under iodide invasion in efficient perovskite solar cells *Science* **377** 1227–31

[25] Jung E H, Jeon N J, Park E Y, Moon C S, Shin T J, Yang T Y and Noh J H 2019 Efficient, stable and scalable perovskite solar cells using poly(3-hexylthiophene) *Nature* **567** 511–5

[26] Zhang H, Xiao J, Shi J, Su H, Luo Y, Li D, Wu H, Chen Y and Meng Q 2018 Self-adhesive macroporous carbon electrodes for efficient and stable perovskite solar cells *Adv. Funct. Mater.* **28** 1802985

[27] Zhang C *et al* 2021 Ti_1–graphene single-atom material for improved energy level alignment in perovskite solar cells *Nat. Energy* **6** 1154–63

[28] Lin Y *et al* 2017 π-Conjugated Lewis base: efficient trap-passivation and charge-extraction for hybrid perovskite solar cells *Adv. Mater.* **29** 1604545

[29] Liu K, Chen S, Wu J, Zhang H, Qin M, Lu X, Tu X, Meng Q and Zhan X 2018 Fullerene derivative anchored SnO_2 for high-performance perovskite solar cells *Energy Environ. Sci.* **11** 3463–71

[30] Jiang Y *et al* 2022 Reducing energy disorder in perovskite solar cells by chelation *J. Am. Chem. Soc.* **144** 5400–10

[31] Zhang M, Dai S, Chandrabose S, Chen K, Liu K, Qin M, Lu X, Hodgkiss J M, Zhou H and Zhan X 2018 High-performance fused ring electron acceptor-perovskite hybrid *J. Am. Chem. Soc.* **140** 14938–44

[32] Eperon G E, Paternò G M, Sutton R J, Zampetti A, Haghighirad A A, Cacialli F and Snaith H J 2015 Inorganic caesium lead iodide perovskite solar cells *J. Mater. Chem.* A **3** 19688–95

[33] Faheem M B, Khan B, Feng C, Farooq M U, Raziq F, Xiao Y and Li Y 2019 All-inorganic perovskite solar cells: energetics, key challenges, and strategies toward commercialization *ACS Energy Lett.* **5** 290–320

[34] Jiang Y, Yuan J, Ni Y, Yang J, Wang Y, Jiu T, Yuan M and Chen J 2018 Reduced-dimensional α-$CsPbX_3$ perovskites for efficient and stable photovoltaics *Joule* **2** 1356–68

[35] Stoumpos C C, Malliakas C D and Kanatzidis M G 2013 Semiconducting tin and lead iodide perovskites with organic cations: phase transitions, high mobilities, and near-infrared photoluminescent properties *Inorg. Chem.* **52** 9019–38

[36] Sutton R J *et al* 2016 Bandgap-tunable cesium lead halide perovskites with high thermal stability for efficient solar cells *Adv. Energy Mater.* **6** 1502458

[37] Zhou Y and Zhao Y 2019 Chemical stability and instability of inorganic halide perovskites *Energy Environ. Sci.* **12** 1495–511

[38] Zhou W, Zhao Y, Zhou X, Fu R, Li Q, Zhao Y, Liu K, Yu D and Zhao Q 2017 Light-independent ionic transport in inorganic perovskite and ultrastable Cs-based perovskite solar cells *J. Phys. Chem. Lett.* **8** 4122–8

[39] Wang P, Zhang X, Zhou Y, Jiang Q, Ye Q, Chu Z, Li X, Yang X, Yin Z and You J 2018 Solvent-controlled growth of inorganic perovskite films in dry environment for efficient and stable solar cells *Nat. Commun.* **9** 2225

[40] Kulbak M, Cahen D and Hodes G 2015 How important is the organic part of lead halide perovskite photovoltaic cells? Efficient $CsPbBr_3$ cells *J. Phys. Chem. Lett.* **6** 2452–6

[41] Wang Y *et al* 2019 Thermodynamically stabilized beta-$CsPbI_3$–based perovskite solar cells with efficiencies >18% *Science* **365** 591–5

[42] Yu B, Shi J, Tan S, Cui Y, Zhao W, Wu H, Luo Y, Li D and Meng Q 2021 Efficient (>20%) and stable all-inorganic cesium lead triiodide solar cell enabled by thiocyanate molten salts *Angew. Chem, Int. Ed.* **60** 13436–43

[43] Yoon S M, Min H, Kim J B, Kim G, Lee K S and Seok S I 2020 Surface engineering of ambient-air-processed cesium lead triiodide layers for efficient solar cells *Joule* **5** 183–96

[44] Wang Y, Zhang T, Kan M and Zhao Y 2018 Bifunctional stabilization of all-inorganic alpha-$CsPbI_3$ perovskite for 17% efficiency photovoltaics *J. Am. Chem. Soc.* **140** 12345–8

[45] Wang Y, Liu X, Zhang T, Wang X, Kan M, Shi J and Zhao Y X 2019 The role of dimethylammonium iodide in $CsPbI_3$ perovskite fabrication: additive or dopant? *Angew. Chem., Int. Ed.* **58** 16691–6

[46] Cui Y *et al* 2022 A versatile molten-salt induction strategy to achieve efficient $CsPbI_3$ perovskite solar cells with a high open-circuit voltage >1.2V *Adv. Mater.* **34** e2205028

[47] Wang J, Che Y, Duan Y, Liu Z, Yang S, Xu D, Fang Z, Lei X, Li Y and Liu S Z 2023 21.15%-efficiency and stable gamma-$CsPbI_3$ perovskite solar cells enabled by an acyloin ligand *Adv. Mater.* **35** e2210223

[48] Chen H, Xiang S, Li W, Liu H, Zhu L and Yang S 2018 Inorganic perovskite solar cells: a rapidly growing field *Solar RRL* **2** 1700188

[49] Byranvand M M, Zuo W, Imani R, Pazoki M and Saliba M 2022 Tin-based halide perovskite materials: properties and applications *Chem. Sci.* **13** 6766–81

[50] Correa-Baena J-P, Saliba M, Buonassisi T, Graetzel M, Abate A, Tress W and Hagfeldt A 2017 Promises and challenges of perovskite solar cells *Science* **358** 739–44

[51] Sun Q and Yin W J 2017 Thermodynamic stability trend of cubic perovskites *J. Am. Chem. Soc.* **139** 14905–8

[52] Steele J A *et al* 2019 Thermal unequilibrium of strained black $CsPbI_3$ thin films *Science* **365** 679–84

[53] Li X, Wu Y, Zhang S, Cai B, Gu Y, Song J and Zeng H 2016 $CsPbX_3$ quantum dots for lighting and displays: room-temperature synthesis, photoluminescence superiorities, underlying origins and white light-emitting diodes *Adv. Funct. Mater.* **26** 2435–45

[54] Yang Z *et al* 2017 Impact of the halide cage on the electronic properties of fully inorganic cesium lead halide perovskites *ACS Energy Lett.* **2** 1621–7

[55] Girisun T C S and Dhanuskodi S 2009 Linear and nonlinear optical properties of tris thiourea zinc sulphate single crystals *Cryst. Res. Technol.* **44** 1297–302

[56] Elbaz G A, Straus D B, Semonin O E, Hull T D, Paley D W, Kim P, Owen J S, Kagan C R and Roy X 2017 Unbalanced hole and electron diffusion in lead bromide perovskites *Nano Lett.* **17** 1727–32

[57] Song J *et al* 2017 Ultralarge all-inorganic perovskite bulk single crystal for high-performance visible-infrared dual-modal photodetectors *Adv. Opt. Mater.* **5** 1700157

[58] Ye T *et al* 2021 Ambient-air-stable lead-free $CsSnI_3$ solar cells with greater than 7.5% efficiency *J. Am. Chem. Soc.* **143** 4319–28

[59] Stoumpos C C, Frazer L, Clark D J, Kim Y S, Rhim S H, Freeman A J, Ketterson J B, Jang J I and Kanatzidis M G 2015 Hybrid germanium iodide perovskite semiconductors: active lone pairs, structural distortions, direct and indirect energy gaps, and strong nonlinear optical properties *J. Am. Chem. Soc.* **137** 6804–19

[60] Huang L Y and Lambrecht W R L 2016 Electronic band structure trends of perovskite halides: beyond Pb and Sn to Ge and Si *Phys. Rev.* B **93** 195211

[61] Jena A K, Kulkarni A and Miyasaka T 2019 Halide perovskite photovoltaics: background, status, and future prospects *Chem. Rev.* **119** 3036–103

[62] Han X *et al* 2019 Lead-free double perovskite Cs_2SnX_6: facile solution synthesis and excellent stability *Small* **15** e1901650

[63] Giustino F and Snaith H J 2016 Toward lead-free perovskite solar cells *ACS Energy Lett.* **1** 1233–40

[64] Slavney A H, Hu T, Lindenberg A M and Karunadasa H I 2016 A bismuth-halide double perovskite with long carrier recombination lifetime for photovoltaic applications *J. Am. Chem. Soc.* **138** 2138–41

[65] Igbari F, Wang Z K and Liao L S 2019 Progress of lead-free halide double perovskites *Adv. Energy Mater.* **9** 1803150

[66] Ma C, Grätzel M and Park N-G 2022 Facet engineering for stable, efficient perovskite solar cells *ACS Energy Lett.* **7** 3120–8

[67] Pradhan N 2021 Why do perovskite nanocrystals form nanocubes and how can their facets be tuned? A perspective from synthetic prospects *ACS Energy Lett.* **7** 92–99

[68] Dong S, Hu Z Y, Wei P, Han J, Wang Z, Liu J, Su B-L, Zhao D and Liu Y 2022 All-inorganic perovskite single-crystal photoelectric anisotropy *Adv. Mater.* **34** e2204342

[69] Tan S *et al* 2022 Temperature-reliable low-dimensional perovskites passivated black-phase $CsPbI_3$ toward stable and efficient photovoltaics *Angew. Chem., Int. Ed.* **61** e202201300

[70] Zhang H *et al* 2023 Tailored cysteine-derived molecular structures towards efficient and stable inorganic perovskite solar cells *Adv. Mater.* e2301140

[71] Liu C, Li W Z, Zhang C L, Ma Y P, Fan J D and Mai Y H 2018 All-inorganic $CsPbI_2Br$ perovskite solar cells with high efficiency exceeding 13% *J. Am. Chem. Soc.* **140** 3825–8

[72] Luo X *et al* 2023 Efficient perovskite/silicon tandem solar cells on industrially compatible textured silicon *Adv. Mater.* **35** e2207883

[73] Ho-Baillie A W Y, Zheng J, Mahmud M A, Fa-Jun M, McKenzie D R and Green M A 2021 Recent progress and future prospects of perovskite tandem solar cells *Appl. Phys. Rev.* **8** 041307

[74] Fu S, Le J, Guo X, Sun N, Zhang W, Song W and Fang J F 2022 Polishing the lead-poor surface for efficient inverted $CsPbI_3$ perovskite solar cells *Adv. Mater.* **34** e2205066

[75] Liang J *et al* 2016 All-inorganic perovskite solar cells *J. Am. Chem. Soc.* **138** 15829–32

[76] Wang H, Liu H, Dong Z, Wei X, Li W, Zhu L, Zhu C, Bai Y and Chen H N 2023 Dimethyl sulfoxide: a promising solvent for inorganic $CsPbI_3$ perovskite *Sci. Bull.* **68** 192–202

[77] Yu B, Zuo C, Shi J, Meng Q and Ding L 2021 Defect engineering on all-inorganic perovskite solar cells for high efficiency *J. Semicond.* **42** 050203

[78] Shockley W and Queisser H J 1961 Detailed balance limit of efficiency of p-n junction solar cells *J. Appl. Phys.* **32** 510–9

[79] Yuan S, Xian Y, Long Y, Cabot A, Li W and Fan J 2021 Chromium-based metal–organic framework as a-site cation in $CsPbI_2Br$ perovskite solar cells *Adv. Funct. Mater.* **31** 2106233

[80] Zhu W, Chai W, Chen D, Ma J, Chen D, Xi H, Zhang J, Zhang C and Hao Y 2021 High-Efficiency (>14%) and air-stable carbon-based, all-inorganic $CsPbI_2Br$ perovskite solar cells through a top-seeded growth strategy *ACS Energy Lett.* **6** 1500–10

[81] Zhou Q, Duan J, Du J, Guo Q, Zhang Q, Yang X, Duan J and Tang Q 2021 Tailored lattice "Tape" to confine tensile interface for 11.08%-efficiency all-inorganic $CsPbBr_3$ perovskite solar cell with an ultrahigh voltage of 1.702 V *Adv. Sci.* **8** e2101418

[82] Liang J *et al* 2019 Defect-engineering-enabled high-efficiency all-inorganic perovskite solar cells *Adv. Mater.* **31** e1903448

[83] Uratani H and Yamashita K 2017 Charge carrier trapping at surface defects of perovskite solar cell absorbers: a first-principles study *J. Phys. Chem. Lett.* **8** 742–6

[84] Ball J M and Petrozza A 2016 Defects in perovskite-halides and their effects in solar cells *Nat. Energy* **1** 16149

[85] Li Y, Zhang C, Zhang X, Huang D, Shen Q, Cheng Y and Huang W 2017 Intrinsic point defects in inorganic perovskite $CsPbI_3$ from first-principles prediction *Appl. Phys. Lett.* **111** 162106

[86] Chen W, Chen H, Xu G, Xue R, Wang S, Li Y and Li Y 2019 Precise control of crystal growth for highly efficient $CsPbI_2Br$ perovskite solar cells *Joule* **3** 191–204

[87] Yu B *et al* 2018 Solvent-engineering toward $CsPb(I_xBr_{1-x})_3$ films for high-performance inorganic perovskite solar cells *J. Mater. Chem.* A **6** 19810–6

[88] Chen C Y, Lin H Y, Chiang K M, Tsai W L, Huang Y C, Tsao C S and Lin H W 2017 All-vacuum-deposited stoichiometrically balanced inorganic cesium lead halide perovskite solar cells with stabilized efficiency exceeding 11% *Adv. Mater.* **29** 1605290

[89] Duan J, Zhao Y Y, He B L and Tang Q W 2018 High-purity inorganic perovskite films for solar cells with 9.72% efficiency *Angew. Chem., Int. Ed.* **57** 3787–91

[90] Chen W, Zhang J, Xu G, Xue R, Li Y, Zhou Y, Hou J and Li Y 2018 A semitransparent inorganic perovskite film for overcoming ultraviolet light instability of organic solar cells and achieving 14.03% efficiency *Adv. Mater.* **30** e1800855

[91] Hutter E M, Sutton R J, Chandrashekar S, Abdi-Jalebi M, Stranks S D, Snaith H J and Sayenije T J 2017 Vapour-deposited cesium lead iodide perovskites: microsecond charge carrier lifetimes and enhanced photovoltaic performance *ACS Energy Lett.* **2** 1901–8

[92] Shi L *et al* 2020 Gas chromatography-mass spectrometry analyses of encapsulated stable perovskite solar cells *Science* **368** 6497

[93] Kulbak M, Gupta S, Kedem N, Levine I, Bendikov T, Hodes G and Cahen D 2016 Cesium enhances long-term stability of lead bromide perovskite-based solar cells *J. Phys. Chem. Lett.* **7** 167–72

[94] Tian J, Wang J, Xue Q, Niu T, Yan L, Zhu Z, Li N, Brabec C J, Yi H L and Cao Y 2020 Composition engineering of all-inorganic perovskite film for efficient and operationally stable solar cells *Adv. Funct. Mater.* **30** 2001764

[95] Li W *et al* 2017 Phase segregation enhanced ion movement in efficient inorganic $CsPbIBr_2$ solar cells *Adv. Energy Mater.* **7** 1700946

[96] Tian J *et al* 2019 Dual interfacial design for efficient $CsPbI_2Br$ perovskite solar cells with improved photostability *Adv. Mater.* **31** e1901152

[97] Zheng K, Ge J, Liu C, Lou Q, Chen X, Meng Y, Yin X, Bu S, Liu C and Ge Z 2021 Improved phase stability of $CsPbI_2Br$ perovskite by released microstrain toward highly efficient and stable solar cells *InfoMat* **3** 1431–44

[98] Zeng Q *et al* 2018 Polymer-passivated inorganic cesium lead mixed-halide perovskites for stable and efficient solar cells with high open-circuit voltage over 1.3 V *Adv. Mater.* **30** 1705393

[99] Xu J *et al* 2022 Stable high-efficiency $CsPbI_2Br$ solar cells by designed passivation using multifunctional 2D perovskite *Adv. Funct. Mater.* **32** 2202829

[100] Swarnkar A, Mir W J and Nag A 2018 Can B-site doping or alloying improve thermal- and phase-stability of all-inorganic $CsPbX_3$ (X = Cl, Br, I) perovskites? *ACS Energy Lett.* **3** 286–9

[101] Wang Q, Zheng X, Deng Y, Zhao J, Chen Z and Huang J 2017 Stabilizing the α-phase of $CsPbI_3$ perovskite by

sulfobetaine zwitterions in one-step spin-coating films *Joule* **1** 371–82
[102] Ghosh D, Ali M Y, Chaudhary D K and Bhattacharyya S 2018 Dependence of halide composition on the stability of highly efficient all-inorganic cesium lead halide perovskite quantum dot solar cells *Sol. Energy Mater. Sol. Cells* **185** 28–35
[103] Li W, Li J, Li J, Fan J, Mai Y and Wang L 2016 Addictive-assisted construction of all-inorganic $CsSnIBr_2$ mesoscopic perovskite solar cells with superior thermal stability up to 473 K *J. Mater. Chem.* A **4** 17104–10
[104] Meng F, Yu B, Zhang Q, Cui Y, Tan S, Shi J, Gu L, Li D, Meng Q and Nan C 2022 Ge incorporation to stabilize efficient inorganic $CsPbI_3$ perovskite solar cells *Adv. Energy Mater.* **12** 2103690
[105] Yang F, Hirotani D, Kapil G, Kamarudin M A, Ng C H, Zhang Y, Shen Q and Hayase S 2018 All-inorganic $CsPb_{1-x}Ge_xI_2Br$ perovskite with enhanced phase stability and photovoltaic performance *Angew. Chem., Int. Ed.* **57** 12745–9
[106] Hu Y, Bai F, Liu X, Ji Q, Miao X, Qiu T and Zhang S 2017 Bismuth incorporation stabilized α-$CsPbI_3$ for fully inorganic perovskite solar cells *ACS Energy Lett.* **2** 2219–27
[107] Jena A K, Kulkarni A, Sanehira Y, Ikegami M and Miyasaka T 2018 Stabilization of α-$CsPbI_3$ in ambient room temperature conditions by incorporating Eu into $CsPbI_3$ *Chem. Mater.* **30** 6668–74
[108] Guo Z, Zhao S, Liu A, Kamata Y, Teo S, Yang S, Xu Z, Hayase S and Ma T 2019 Niobium incorporation into $CsPbI_2Br$ for stable and efficient all-inorganic perovskite solar cells *ACS Appl Mater. Interfaces* **11** 19994–20003
[109] Zhao X, Liu T, Burlingame Q C, Liu T, Holley R, Cheng G, Yao N, Gao F and Loo Y L 2022 Accelerated aging of all-inorganic, interface-stabilized perovskite solar cells *Science* **377** 307–10
[110] Li B, Zhang Y, Fu L, Yu T, Zhou S, Zhang L and Yin L 2018 Surface passivation engineering strategy to fully-inorganic cubic $CsPbI_3$ perovskites for high-performance solar cells *Nat. Commun.* **9** 1076
[111] Zhao B *et al* 2018 Thermodynamically stable orthorhombic gamma-$CsPbI_3$ thin films for high-performance photovoltaics *J. Am. Chem. Soc.* **140** 11716–25
[112] Zhang J, Fang Y, Zhao W, Han R, Wen J and Liu S Z 2021 Molten-salt-assisted $CsPbI_3$ perovskite crystallization for nearly 20%-efficiency solar cells *Adv. Mater.* **33** e2103770
[113] Liu C *et al* 2018 Structurally reconstructed $CsPbI_2Br$ perovskite for highly stable and square-centimeter all-inorganic perovskite solar cells *Adv. Energy Mater.* **9** 1803572
[114] Jiang Q, Zhang L, Wang H, Yang X, Meng J, Liu H, Yin Z, Wu J, Zhang X and You J 2016 Enhanced electron extraction using SnO_2 for high-efficiency planar-structure $HC(NH_2)_2PbI_3$-based perovskite solar cells *Nat. Energy* **2** 1–7
[115] Jiang Q, Zhang X and You J 2018 SnO_2: a wonderful electron transport layer for perovskite solar cells *Small* **14** e1801154
[116] Ye Q, Zhao Y, Mu S, Ma F, Gao F, Chu Z, Yin Z, Gao P, Zhang X and You J 2019 Cesium lead inorganic solar cell with efficiency beyond 18% via reduced charge recombination *Adv. Mater.* **31** e1905143
[117] Zhang T *et al* 2022 Ion-modulated radical doping of spiro-OMeTAD for more efficient and stable perovskite solar cells *Science* **377** 495–501
[118] Yuan J *et al* 2018 Band-aligned polymeric hole transport materials for extremely low energy loss α-$CsPbI_3$ perovskite nanocrystal solar cells *Joule* **2** 2450–63
[119] Li M H *et al* 2021 Electrical loss management by molecularly manipulating dopant-free poly(3-hexylthiophene) towards 16.93% $CsPbI_2Br$ solar cells *Angew. Chem., Int. Ed.* **60** 16388–93
[120] Liang J, Zhao P, Wang C, Wang Y, Hu Y, Zhu G, Ma L, Liu J and Jin Z 2017 $CsPb_{0.9}Sn_{0.1}IBr_2$ based all-inorganic perovskite solar cells with exceptional efficiency and stability *J. Am. Chem. Soc.* **139** 14009–12
[121] Heo J H, Zhang F, Park J K, Joon Lee H, Lee D S, Heo S J, Luther J M, Berry J J, Zhu K and Im S H 2022 Surface engineering with oxidized $Ti_3C_2T_x$ MXene enables efficient and stable p-i-n-structured $CsPbI_3$ perovskite solar cells *Joule* **6** 1672–88